Astronomy & Astrophysics manuscript no. output
June 6, 2023

A method to deconvolve stellar profiles

The Non-Rotating Line utilizing Gaussian Sum Approximation.

P. Escárate[1], M. Curé[2], I. Araya[3], M. Coronel[1], A.L. Cedeño[4], L. Celedon[2], J. Cavieres[5], J.C. Agüero[4], C. Arcos[2], L. S. Cidale[6,7], R. S. Levenhagen[8], R. Pezoa[9], and S. Simón-Díaz[10,11]

[1] Escuela de Ingeniería Eléctrica, Facultad de Ingeniería, Pontificia Universidad Católica de Valparaíso, Valparaíso, Chile. e-mail: pedro.escarate@pucv.cl
[2] Instituto de Física y Astronomía, Facultad de Ciencias, Universidad de Valparaíso, Valparaíso, Chile. e-mail: michel.cure@uv.cl
[3] Centro de Óptica e Información Cuántica, Vicerrectoría de Investigación, Universidad Mayor, Santiago, Chile
[4] Electronics Engineering Department, Universidad Técnica Federico Santa María, Valparaíso, Chile.
[5] Department of Geography, University of Bayreuth, Germany
[6] Departamento de Espectroscopía, Facultad de Ciencias Astronómicas y Geofísicas, Universidad Nacional de La Plata (UNLP),
[7] Instituto de Astrofísica La Plata, CCT La Plata, CONICET-UNLP, Paseo del Bosque S/N, 1900 La Plata, Argentina
[8] Departamento de Física, Universidade Federal de Sao Paulo, Rua Prof. Artur Riedel, 275, 09972-270, Diadema, SP, Brazil
[9] Departmento de Informática, Universidad Técnica Federico Santa María, Valparaíso, Chile
[10] Universidad de La Laguna, Departamento de Astrofísica, 38206 La Laguna, Tenerife, Spain
[11] Instituto de Astrofísica de Canarias, Avenida Vía Láctea s/n, 38205 La Laguna, Tenerife, Spain

Received ; accepted

ABSTRACT

Context. Nowadays, one of the standard procedures to determine stellar and wind parameters of massive stars is to compare the observed spectral lines with a grid of synthetic lines. These synthetic lines are calculated using NLTE radiative transfer codes.
Aims. In this standard procedure, after estimating the stellar projected rotational speed ($v \sin i$), all synthetic models need to be convolved using this value to perform the comparison with the observed line and estimate the stellar parameters.
Methods. In this work, we propose a methodology to deconvolve the observed line profile to one from a *non-rotating* star. Thus, to perform the comparison, we do not need to convolve all the synthetic profiles, sparing them significant time resources. This is a challenging inverse problem and our proposed deconvolution method is based on transforming this inverse problem into an optimization of a direct problem. We propose to use a Gaussian Sum Approximation (GSA) to obtain the line profile without the broadening effect due to stellar rotation. After selecting the most adequate model to derive the fundamental GSA'a parameters, we convolve it with the known $v \sin i$ to obtain the profile considering the $v \sin i$. Finally, we compare this approximated line profile directly with the observed spectrum.
Results. The performance of the proposed method is analyzed using synthetic and observed lines. The results show that the proposed deconvolution method yields accurate non-rotating profiles.
Conclusions. The proposed approach with Gaussian Sum Approximation is an accurate method to deconvolve spectral lines.

Key words. stars: rotation – methods: Maximum Likelihood – methods: Gaussian approximation – stars: rotation

1. Introduction

Estimating the physical properties and chemical composition of massive stars is essential to describe their wind hydrodynamics (Curé & Araya 2023), and their evolutionary status (Kudritzki & Puls 2000; Puls et al. 2008; Vink 2022), and quantitative stellar spectroscopy is a powerful tool for determining these parameters. Based on a comparison metric, this technique compares the observed spectral lines with a set of synthetic ones. These synthetic line profiles are created using a stellar atmosphere code that best suits the analysis of the star under study. However, to perform the spectral fitting, it is necessary to consider the line-broadening effect produced by the stellar rotation.

In the latter years, automated fitting techniques to carry out this quantitative spectroscopy analysis have been developed to analyze large samples of stellar spectra (see, e.g., Mokiem et al. 2005; Lefever et al. 2010; Simón-Díaz et al. 2011; Brands et al. 2022). These techniques have gradually replaced the traditional but time-consuming naked-eye method due to the large multi-parameter space to be explored in the analysis. One of the main steps to perform a quantitative spectroscopic analysis is the determination of the line-broadening parameters (Simón-Díaz 2020). The Fourier Transform method (Carroll 1933) is one of the most used to derive the projected rotational velocities ($V \sin i$, where V is the equatorial linear velocity and i is the inclination angle of the stellar rotation axis with respect to the observer) from stellar observed lines. However, this is not the only line-broadening mechanism in stars; e.g., thermal, radiative, collisional, microturbulent, and macroturbulent broadenings are also present in massive stars; many of them are already considered in stellar atmosphere radiative transfer calculations.

To estimate the physical parameters (e.g., $T_{\rm eff}$, $\log g$) of a star in the frame of quantitative spectroscopy, the non-rotating synthetic line profiles are rotationally convolved and then compared

with the observed lines. The convolution is performed after measuring $V \sin i$ and the macro-turbulence speed (see e.g., Simón-Díaz 2020; Zorec 2023, and references therein).

Nowadays, there are many synthetic line spectra libraries that can be used to compare with the observed spectra, but all the models from the subset of selected synthetic spectra must be rotationally convolved to proceed with the comparison, and this is a very CPU-time-consuming task.

Instead of convolving a large number of synthetic models, in this work, we propose a method to obtain the non-rotating observed spectral line ("deconvolved spectrum"). Using this non-rotating "observed" line spectrum, we can compare it with the non-rotating synthetic spectra and select the best atmospheric model. Then, we rotationally convolve that model to fit the "real" observation.

This is a very interesting *inverse problem* and was the focus of the work of Carroll (1933). Standard tools such as, e.g., Tihkonov (or Ridge) regularization (see, e.g. Christen et al. 2016), cannot be applied because now the unknown function is the *kernel* of the integral expression. Alternatively, instead of solving this inverse problem, we propose to *optimize a direct problem* using a Gaussian Sum Approximation (GSA) of the kernel in the integral problem.

The method used in this paper is based on Carvajal et al. (2018), where a general estimation algorithm is developed using data augmentation. In this work, we adapt the proposed method in Carvajal et al. (2018); Orellana, R. et al. (2019); Christen et al. (2016) to estimate the non-rotational spectra.

This article is structured as follows: Section 2 provides the mathematical description of the proposed method. Then, in Section 3, Monte Carlo simulations of the proposed method applied to synthetic spectral lines are presented to show the robustness of this method. Next, in Section 4, some observed spectral lines are deconvolved. Finally, in Section 5, discussions and the final remarks are presented.

2. Effect of rotation in spectral lines

The rotational convolution of the non-rotating star profile $I(\zeta)$ satisfies the following integral equation for a spectral line, first described by Carroll (1933) as:

$$O(\zeta) = K_N \int_{-1}^{1} I(\zeta + \beta x)\, g(x)\, dx, \tag{1}$$

where K_N is a normalization factor, $\beta = V \sin i/c$ is the rotational velocity, i is the inclination angle, c is the speed of light, and $g(x)$ represents the rotational profile which depends on the assumed limb-darkening law (see Levenhagen 2014). A summary of four different limb-darkening laws is given in Appendix A. The variable ζ is defined as:

$$\zeta = \frac{\lambda - \lambda_m}{\lambda_m}, \tag{2}$$

being λ the wavelength, and λ_m the wavelength of the centre of the line.

3. Gaussian Sum Approximation approach (GSA)

Knowing the β parameter, and a rotational profile, $g(x)$, the inverse problem consists in finding the non-rotational spectral line $I(\zeta)$ from the observed data $O(\zeta)$.

In this work, we propose to approximate the unknown spectral line $I(\zeta)$ by a GSA (Wiener 1932), namely:

$$\hat{I}(\zeta|\theta) \approx \sum_{j=1}^{N} \gamma_j \mathcal{N}(\zeta; \mu_j, \sigma_j^2), \tag{3}$$

where $N \in \mathbb{N}$ represents the number of Gaussian functions used to approximate the spectral line, $\gamma_j \in \mathbb{R}$ represents the jth weight, and $\mathcal{N}(\zeta; \mu_j, \sigma_j^2)$ represents a Gaussian function given by:

$$\mathcal{N}(\zeta; \mu_j, \sigma_j^2) = \frac{1}{\sqrt{2\pi\sigma_j^2}} \exp\left\{-\frac{1}{2}\frac{(\zeta - \mu_j)^2}{\sigma_j^2}\right\}, \tag{4}$$

here σ_j is a measure of the width of the jth Gaussian function with center μ_j. Thus, the parameters to estimate are given by the vector:

$$\theta = [\gamma_1, \mu_1, \sigma_1^2 ...., \gamma_N, \mu_N, \sigma_N^2], \tag{5}$$

Then, replacing Eq. (3) in Eq. (1) we obtain:

$$\begin{aligned}\hat{O}(\zeta|\theta) &\approx K_N \int_{-1}^{1} \hat{I}(\zeta + \beta x|\theta)\, g(x)\, dx, \\ &\approx K_N \sum_{j=1}^{N} \int_{-1}^{1} \gamma_j\, \mathcal{N}(\zeta + \beta\, t; \mu_j, \sigma_j^2)\, g(x)\, dx.\end{aligned} \tag{6}$$

The integral in Eq. (6) is computed by utilising Gauss-Legendre numerical integration technique, see, e.g., Cohen (2011), namely:

$$\hat{O}(\zeta|\theta) \approx K_N \sum_{j=1}^{N} \sum_{k=1}^{K} \gamma_j\, \omega_k\, \mathcal{N}(\zeta + \beta\, \phi_k;\, \mu_j, \sigma_j^2)\, g(\phi_k), \tag{7}$$

where ω_k and ϕ_k are weights and zeros of the Kth order Legendre polynomials defined by the quadrature rule. On the other hand, in this work, we assume that the available measurements of $O_M(\zeta_\tau)$ $(\tau = 1, ..., M)$ are contaminated by measurement noise, as follows:

$$O_M(\zeta_\tau) = O(\zeta) + w_\tau, \tag{8}$$

where w_τ is zero-mean Gaussian white noise with variance σ^2. In addition, we assume that the observations are independent and identically distributed. Thus, the probability of the observed measurement $O_M(\zeta_\tau)$ is given by:

$$\mathcal{N}(O_M(\zeta_\tau); \hat{O}(\zeta_\tau|\theta), \sigma^2) = \frac{1}{\sqrt{2\pi\sigma^2}} \exp\left\{-\frac{1}{2}\frac{(O_M(\zeta_\tau) - \hat{O}(\zeta_\tau|\theta))^2}{\sigma^2}\right\}. \tag{9}$$

Then, the likelihood function that represents the probability of the set of measurements is given by:

$$\begin{aligned}L_M(\theta) &= \prod_{\tau=1}^{M} \mathcal{N}(O_M(\zeta_\tau); \hat{O}(\zeta_\tau|\theta), \sigma^2), \\ &= \prod_{\tau=1}^{M} \frac{1}{\sigma\sqrt{2\pi}} \exp\left\{-\frac{1}{2}\frac{(O_M(\zeta_\tau) - \hat{O}(\zeta_\tau|\theta))^2}{\sigma^2}\right\}.\end{aligned} \tag{10}$$

The log-likelihood function $\ell_M(\theta) = \log\{L_M(\theta)\}$ reads:

$$\ell_M(\theta) = \log\left\{\prod_{\tau=1}^{M}\frac{1}{\sigma\sqrt{2\pi}}\exp\left\{-\frac{1}{2}\frac{(O_M(\zeta_\tau)-\hat{O}(\zeta_\tau|\theta))^2}{\sigma^2}\right\}\right\},$$
$$= -\frac{M}{2}\log\left\{\sigma^2\right\} - \frac{M}{2}\log\{2\pi\} - \frac{1}{2\sigma^2}\sum_{\tau=1}^{M}(O_M(\zeta_\tau)-\hat{O}(\zeta_\tau|\theta))^2. \tag{11}$$

Then, concentrating the log-likelihood function in the parameter vector θ, we obtain the following (Gouriéroux & Monfort 1989):

$$\ell_M(\theta) = -\frac{M}{2}\log\left\{\frac{1}{M}\sum_{\tau=1}^{M}(O_M(\zeta_\tau)-\hat{O}(\zeta_\tau|\theta))^2\right\} - \frac{M}{2}. \tag{12}$$

Since $\log\{\cdot\}$ is a monotonic function and neglecting the constant terms in Eq. (12), we obtain the following concentrated function of θ:

$$\mathcal{J}(\theta) = \frac{1}{M}\sum_{\tau=1}^{M}(O_M(\zeta_\tau)-\hat{O}(\zeta_\tau|\theta))^2. \tag{13}$$

Thus, the following optimization problem is solved in order to get the deconvolved spectra $\hat{I}(\zeta|\theta)$:

$$\hat{\theta} = \arg\min_{\theta}\mathcal{J}(\theta). \tag{14}$$

The minimization problem, Eq. (14), is solved using the MATLAB function '*fmincon*,' setting the '*sqp*' algorithm, the "*Max Function Evaluations*' parameter at 5000, and '*Max Iterations*' parameter at 100000.

We summarize our proposed deconvolution algorithm in Table 1.

Table 1. Proposed algorithm

Step 1: Set a random initial value θ^0.
Step 2: Compute $\hat{I}(\zeta\|\theta^0)$ as in Eq. (3).
Step 3: Compute $\hat{O}(\zeta\|\theta^0)$ as in Eq. (7).
Step 4: Minimize $\mathcal{J}(\theta)$ to find $\hat{\theta}$.
Step 5: Compute the deconvolved spectra $\hat{I}(\zeta\|\hat{\theta})$.

4. Simulations

In this section, we present Monte Carlo (MC) numerical simulations to assess the performance of the proposed direct problem optimization.

The synthetic data $O(\zeta_1), O(\zeta_2), ..., O(\zeta_M)$ were generated convolving a synthetic non-rotating spectral line, $I(\zeta)$, in Eq. (1). The synthetic non-rotating lines were calculated using the plane-parallel Non-Local Thermodynamic Equilibrium (NLTE) Tlusty[1] code (Hubeny & Lanz 1995). We compute a model with $T_{\rm eff}$ = 30 000 K and $\log g$ = 4, with solar abundance and a resolution of 0.01 Å in the range of 4500 and 4600Å.

The simulation setup is the following:

1) Three values of Gaussian functions $N = \{10, 20, 30\}$ were considered.
2) K = 30 points (ω_k, ϕ_k) of the Gauss-Legendre quadrature were considered to solve the integral in Eq. (6).
3) Three values of $V \sin i = \{50, 100, 200\}$ km s^{-1} were considered.
4) The number of MC simulations is $n_{\rm MC}$ = 200.
5) Linear limb-darkening ($\epsilon = 0.6$, $\omega = 0$) .

Although linear limb-darkening was used in the simulations, the proposed method could be used with other limb-darkening laws.

4.1. Estimation using GSA

In order to evaluate the performance of the deconvolution method, a synthetic absorption spectral line was approximated using the proposed algorithm with three different values of Gaussian functions $N = \{10, 20, 30\}$. In this case we adopted the He I λ4471 Å line.

The accuracy of the deconvolution was assessed by comparing the approximated absorption spectral lines with the original synthetic absorption line.

Figure 1 shows the absorption spectral lines approximated using $N = \{10, 20, 30\}$ Gaussian functions, respectively. The solid blue line represents the original synthetic absorption line, while the dotted red line is the GSA that represents the best of 200 MC simulations.

It was found that the root mean square error (RMSE) between the original synthetic absorption line and the GSA was greater for N = 10 and N = 30 compared to N = 20. The best RMSE was obtained for N = 20, then the subsequent analysis in the following sections was conducted using N = 20 Gaussian functions. This choice represents the optimal balance between RMSE and computational time. The results demonstrate that the proposed deconvolution method accurately approximates the synthetic spectral line.

4.2. Deconvolving Synthetic profiles

In order to evaluate the performance of the proposed method, three values of $V \sin i = \{50, 100, 200\}$ km s^{-1} were considered. Absorption lines were examined for each case. The results are presented in Fig. 2, which shows the GSA of the spectral lines with $V \sin i = \{50, 100, 200\}$ km s^{-1}. It is worth noting that for each $V \sin i$ case, the proposed method exhibits an excellent agreement between the true deconvolution (solid blue line) and the deconvolution estimated by the proposed method (dotted red line). This indicates that the proposed method is robust and accurate in deconvolving spectra with different $V \sin i$ values. Furthermore, the results suggest that the proposed method can be a reliable tool for analysing observed spectra. However, it is important to note that the "non-rotating spectra" obtained through line deconvolution of rapidly rotating objects should be treated as an initial approximation. Figure 2(c) illustrates that the RMSE changes according to the value of $V \sin i$. Moreover, increasing the number of Gaussian functions N utilized in the GSA, as demonstrated in Fig. 1, can effectively reduce the RMSE of the difference.

5. Deconvolving real profiles

In this section, we apply the proposed method to He I λ4471 Å and Si III λ4552 Å lines from three stars: HD 115842, HD 47240, and HD 206267. These objects were selected to test the method's performance.

[1] http://tlusty.oca.eu

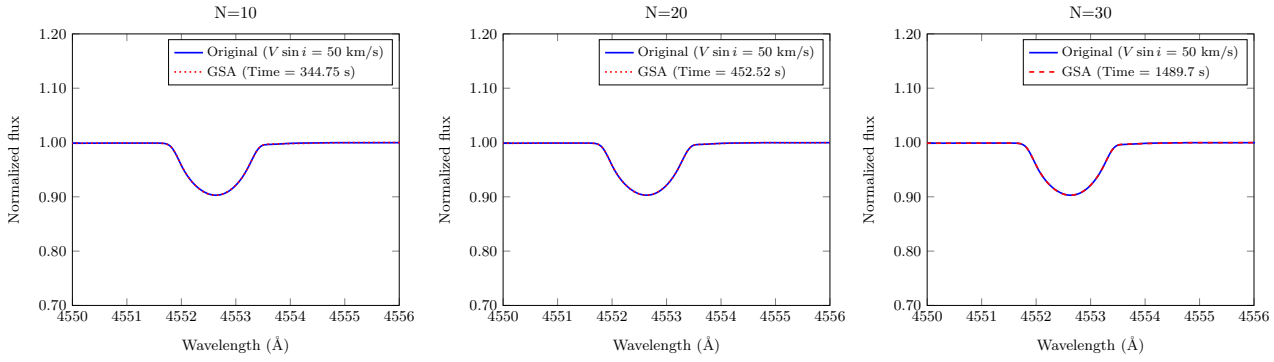

(a)

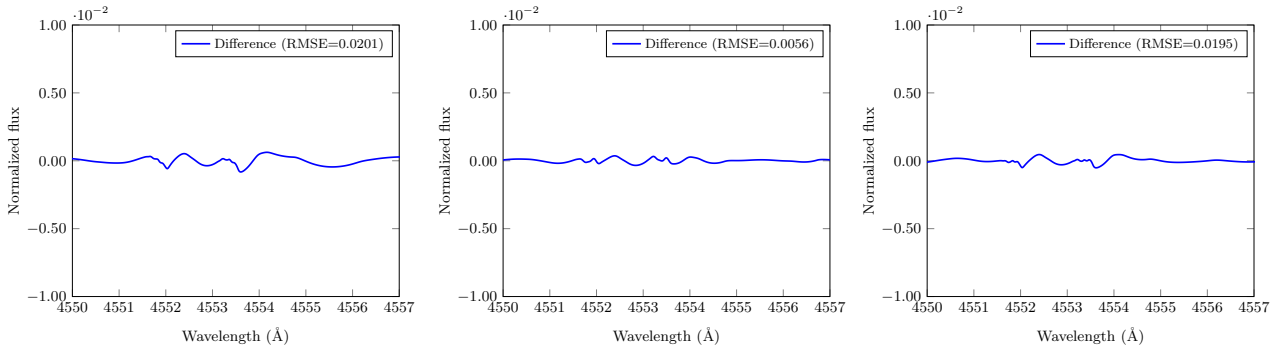

(b)

Fig. 1. Absorption spectral line GSA for N = 10, 20 and 30 Gaussian functions: (a) The solid blue line represents the synthetic profile, and the dotted red line represents the best GSA of 200 MC simulations. (b) The solid blue line represents the difference between the synthetic profile and the GSA.

The Iacob-broad tool described in Simón-Díaz, S. & Herrero, A. (2014) is utilized for estimating the rotational velocity ($V \sin i$) and the macroturbulent velocity (V_{mac}) through a combined methodology of Fourier transform (FT) and goodness-of-fit (GOF). This tool provides four different estimations of $V \sin i$: the $V \sin i$ value corresponding to the first zero of the FT (red value), the $V \sin i$ and V_{mac} obtained from the GOF when both are treated as independent parameters (blue value), the $V \sin i$ resulting from the GOF when V_{mac} is fixed at zero (green value), and the V_{mac} resulting from the GOF when the $V \sin i$ is fixed at the value corresponding to the first zero of the FT (magenta value). In this work, we utilize the $V \sin i$ corresponding to the first zero of the FT (red value), as estimated by the Iacob-broad tool, to perform the deconvolution of the spectra. The specific values obtained for the stars can be found in Appendix B, C and D.

The spectra of HD 115842 and HD 47240 were obtained from Haucke et al. (2018), and the observations of these stars were made using the REOSC spectrograph in cross-dispersion mode, which was equipped on the Jorge Sahade 2.15 m telescope at the Complejo Astronomico El Leoncito (CASLEO), San Juan, Argentina. The spectra of HD 206267 were obtained from Nakano et al. (2012); Wojdowski et al. (2002). By applying the proposed method to these observed line profiles of stars, the study aims to determine its effectiveness and accuracy in deconvolving real observed spectra.

5.1. HD 115842 star

The star HD 115842 is classified as a B0.5 Ia spectral type with a rotational velocity of $V \sin i$ = 63.5 km s^{-1}, determined using the Iacob-broad tool on the Si III line (Appendix B). The spectral lines He I λ4471 Å, and Si III λ4552 Å in Fig. 3 are absorption lines. The upper panel of Fig. 3 shows He I λ4471 Å and Si III λ4552 Å lines as a solid blue line and the GSA as a dotted red line. The GSA represents the mean of 200 MC simulations. In the lower panel of Fig. 3, the estimated deconvolution spectra of each line are displayed as a solid blue line, with the dotted red lines representing the 95.44% confidence interval ($\mu - 2\sigma$, $\mu + 2\sigma$). The deconvolution process for each spectral line was carried out using the proposed method. The results suggest that the proposed method effectively estimates the deconvolved spectra of several spectral lines.

5.2. HD 47240 star

HD 47240 is a B1 Ib star with a spectral type catalogued by Turner (1976) and a rotational velocity of $V sini$ = 106.0 km s^{-1}, determined using the Iacob-broad tool on the Si III line (Appendix C). Figure 4 (upper panel) displays the He I and Si III absorption lines as solid blue lines and the GSA as a dotted red line, following the same procedure as in the HD 115842 analysis, the GSA represents the mean of 200 MC simulations. The lower panel of Fig. 4 presents the estimated deconvolution spectra for each line as a solid blue line, while the dotted red lines represent the 95.44% confidence interval. The results indicate the effectiveness of the proposed method in accurately deconvolving observed spectra of both He I and Si III absorption lines.

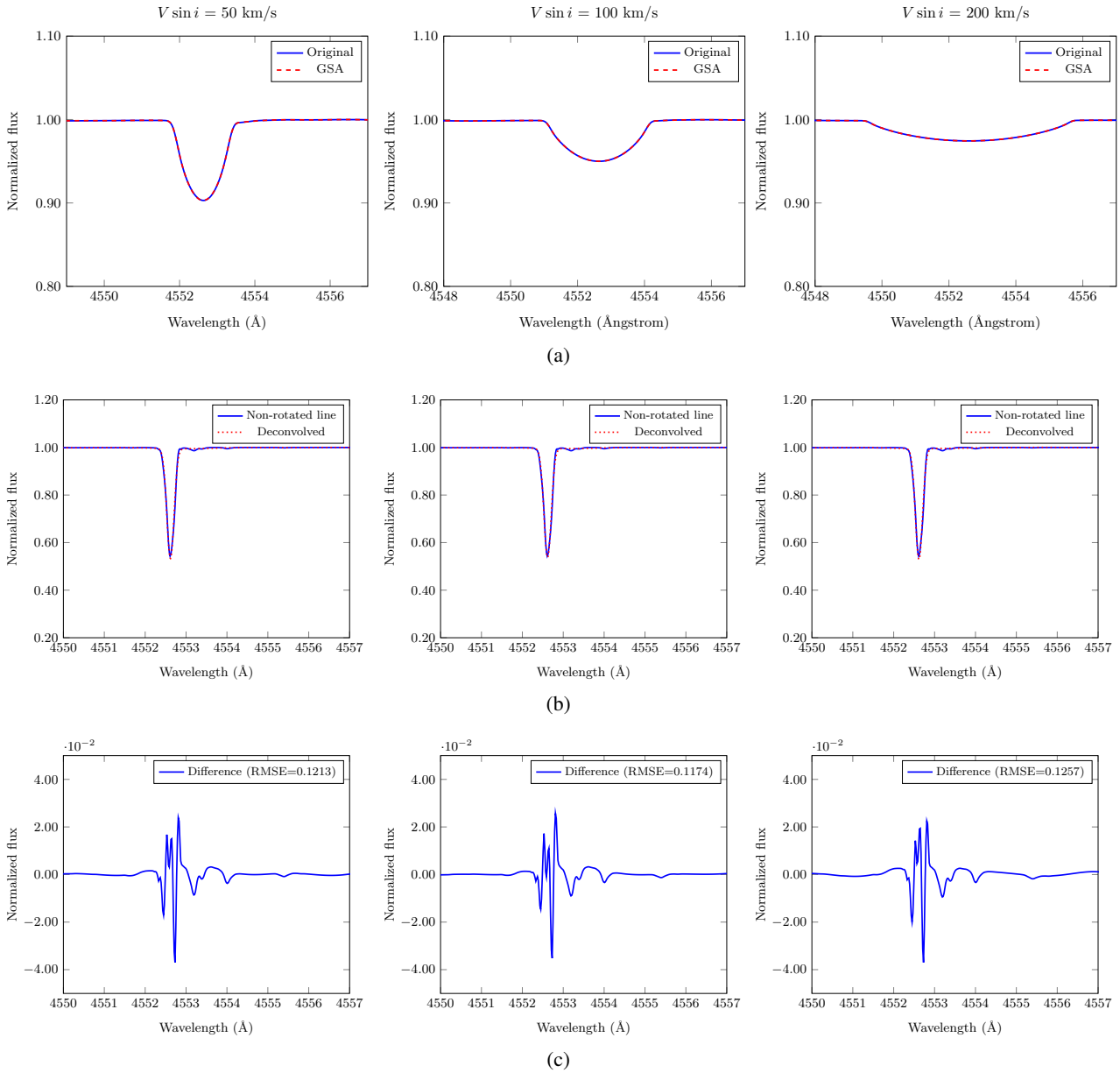

Fig. 2. Absorption spectral line for $V \sin i = \{50, 100, 200\}$ km s^{-1}: (a) The solid blue line represents the synthetic profile and the dotted red line represents the best GSA of 200 MC simulations. (b) The solid blue line represents the non-rotated line, and the dotted red line represents the deconvolved line. (c) The solid blue line represents the difference between the non-rotated line and the deconvolved line.

5.3. HD 206267 star

HD 206267 has a spectral type O6 (Nakano et al. 2012; Wojdowski et al. 2002) and a rotational velocity of $V \sin i = 186.6$ km s^{-1}, determined using the Iacob-broad tool on the Si III line (Appendix D). The upper panel of Fig. 5 shows the observed He I and Si III spectral absorption lines as a solid blue line and the GSA as a dotted red line. As with the previous figures, the GSA represents the mean of 200 MC simulations. In the lower panel, the deconvolution of each line is shown as a solid blue line, with the dotted red lines indicating the 95.44% confidence interval. Despite the presence of measurement noise in the He I and Si III lines, the proposed method is effective in estimating the deconvolved spectra of both He I and Si III lines, as the results demonstrate. The deconvolved spectra shown in Fig. 5 exhibit spurious peaks caused by the noise in the original spectra, with a signal-to-noise ratio $S/R = 74$. Consequently, we highly recommend utilizing the proposed method for spectra with an S/R greater than 150.

6. Discussion and Conclusions

This work presents a novel application for estimating the non-rotating (deconvolved) line spectra based on GSA. The proposed method uses a known rotational velocity ($V \sin i$) obtained from the Iacob-broad tool. It can directly estimate the non-rotating spectral line ($\hat{I}(\zeta)$) from the observed one ($\hat{O}(\zeta|\theta)$) without requiring any intermediate steps or smoothing techniques. It is worth noting that the GSA method is computationally efficient, taking a few minutes to obtain the deconvolved spectral line. However, the rotational profiles described in Appendix A do not take into account either the gravitational darkening or the stellar geometrical deformation due to high rotation (von Zeipel 1924;

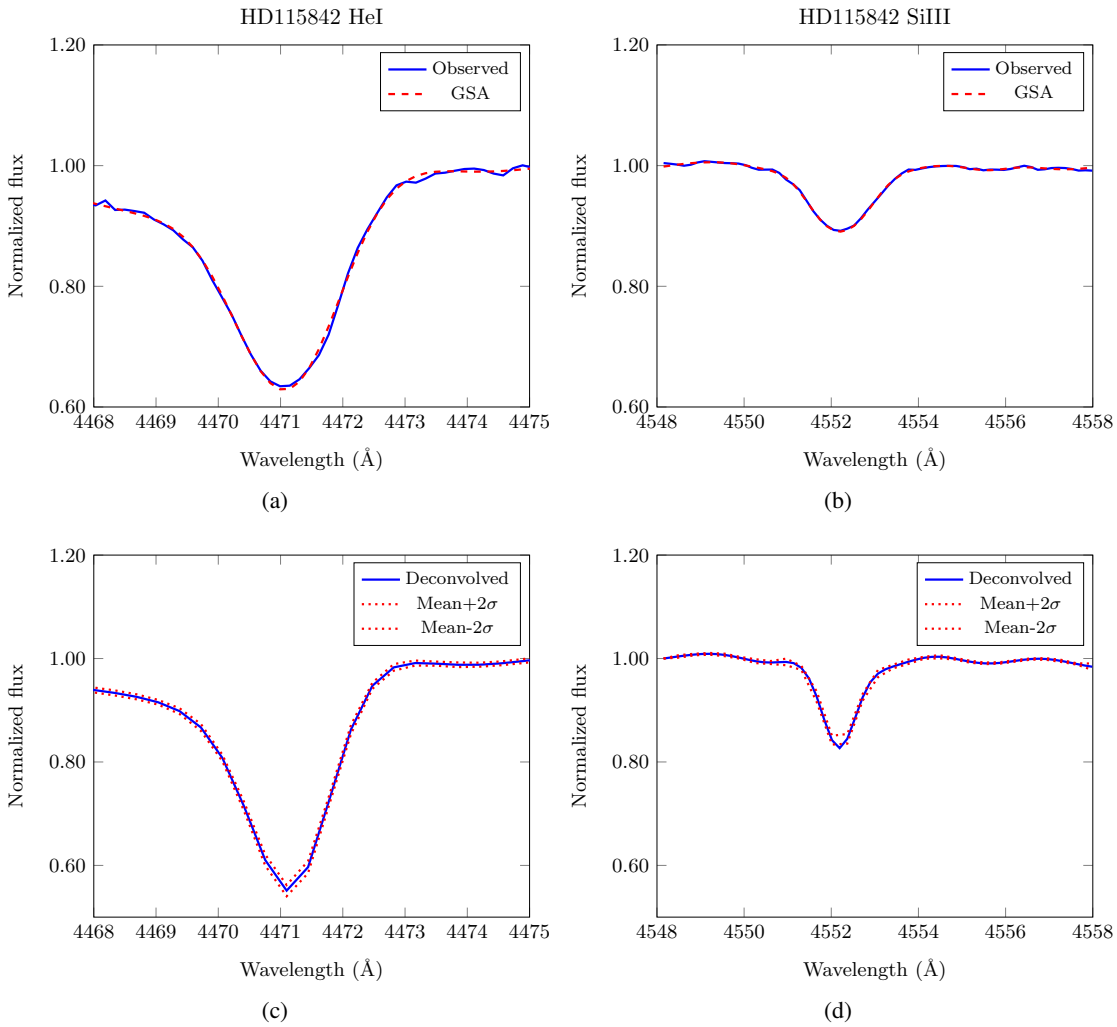

Fig. 3. Deconvolution of two absorption lines for the star HD 115842: (a) The solid blue line represents the observed He I λ 4471 Å line and the dotted red line represents the mean GSA. (b) The solid blue line represents the observed Si III λ 4552 Å line and the dotted red line represents the mean GSA. (c) The solid blue line represents the deconvolved He I line and the dotted red lines representing the confidence interval. (d) The solid blue line represents the deconvolved Si III line and the dotted red lines represent the confidence interval.

Espinosa Lara & Rieutord 2011). Therefore, the method should be safely used for non-highly rotating stars.

To evaluate the effectiveness of the proposed method, we conducted an analysis using synthetic and observed lines, considering different spectral lines and numbers of Gaussian functions in the GSA ($N = \{10, 20, 30\}$). We found that the proposed method accurately deconvolves the spectral observed line, even in the presence of a high level of noise. However, we recommend using observed spectra with a $S/N > 150$ in order to avoid spurious peaks.

Summarising, the proposed method successfully estimates non-rotating line spectra using GSA, even in the presence of noise. In addition, this method can effectively deconvolve different spectral lines employing a selected limb darkening law.

Acknowledgements. This work was partially supported by VINCI-DI PUCV through grant No 039.315/2023. J.C. Agüero and M. Coronel thank the support from ANID-Fondecyt project 1211630 and 3230398 and the Advanced Center for Electrical and Electronic Engineering (AC3E, Proyecto Basal FB0008). M. Curé, C. Arcos & I. Araya thanks the support from ANID-Fondecyt project 1230131 and the continuous support from Centro de Astrofísica de Valparaíso and Centro de Estudios Atmosféricos y Astroestadística (CEAAS), Universidad de Valparaíso. Lydia S. Cidale acknowledges the financial support from CONICET (PIP 1337) and Universidad Nacional de La Plata (Programa de Incentivos 11/G160), Argentina. This project has received funding from the European Union's Framework Programme for Research and Innovation Horizon 2020 (2014-2020) under the Marie Skłodowska-Curie Grant Agreement No. 823734.

References

Brands, S. A., de Koter, A., Bestenlehner, J. M., et al. 2022, A&A, 663, A36
Carroll, J. A. 1928, MNRAS, 88, 548
Carroll, J. A. 1933, MNRAS, 93, 478
Carvajal, R., Orellana, R., Katselis, D., Escárate, P., & Agüero, J. C. 2018, PLOS ONE, 13, 1
Christen, A., Escárate, P., Curé, M., Rial, D. F., & Cassetti, J. 2016, Astronomy & Astrophysics, 595, 1
Cohen, H. 2011, Numerical Approximation Methods: Π ≈ 355/113 (Springer)
Curé, M. & Araya, I. 2023, Galaxies, 11, 68
Espinosa Lara, F. & Rieutord, M. 2011, Astronomy & Astrophysics, 533, A43
Gouriéroux, C. & Monfort, A. 1989, Statistique et modèles économétriques, English translation (1995), Vol. 1 (Cambridge University Press)
Haucke, M., Cidale, L. S., Venero, R. O. J., et al. 2018, A&A, 614, A91
Hubeny, I. & Lanz, T. 1995, The Astrophysical Journal, 439, 875
Kudritzki, R.-P. & Puls, J. 2000, Annual Review of Astronomy and Astrophysics, 38, 613
Lefever, K., Puls, J., Morel, T., et al. 2010, Astronomy & Astrophysics, 515, A74
Levenhagen, R. S. 2014, The Astrophysical Journal, 797, 29
Mokiem, M. R., de Koter, A., Puls, J., et al. 2005, Astronomy & Astrophysics, 441, 711

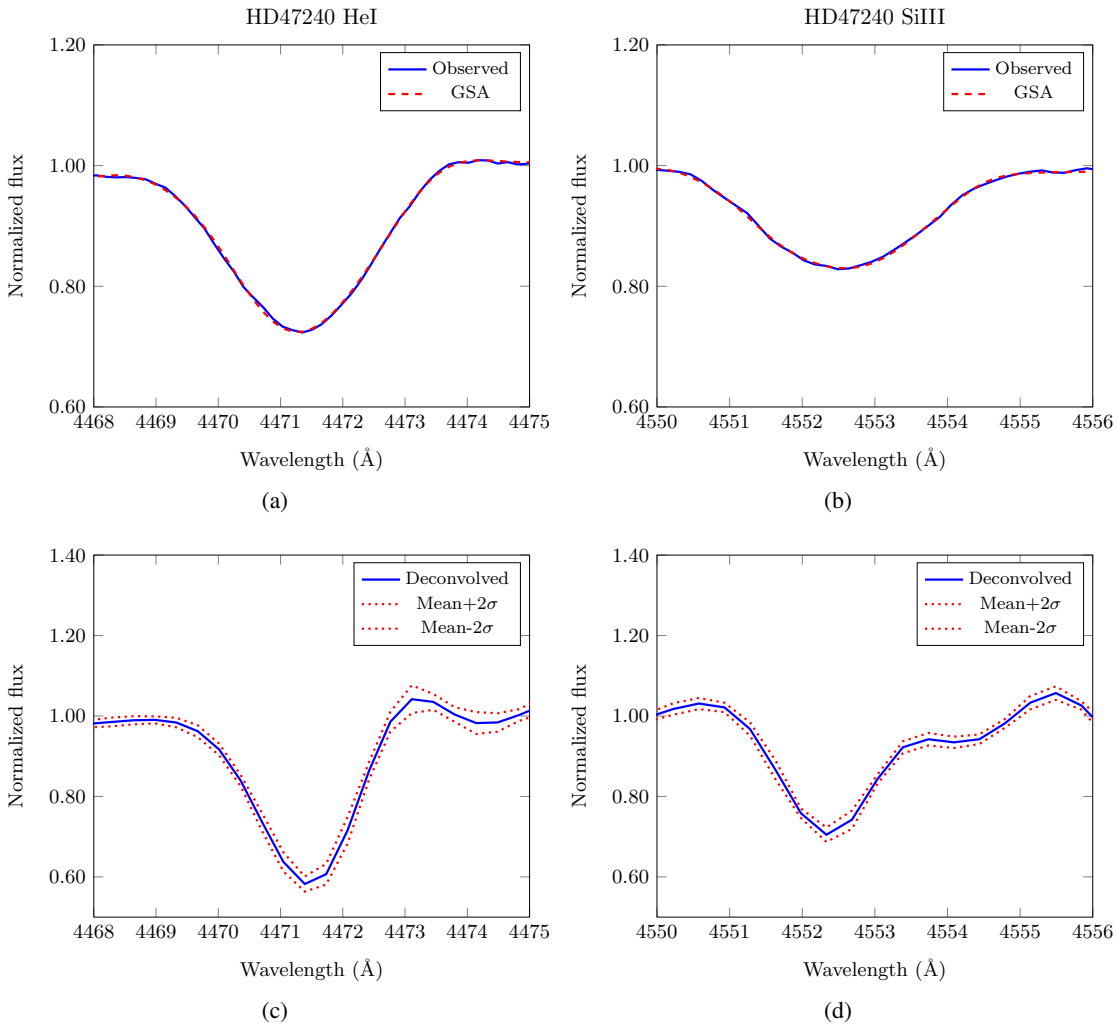

Fig. 4. Deconvolution of two absorption lines for the star HD 47240: (a) The solid blue line represents the observed of He I spectral line, and the dotted red line represents the mean GSA. (b) The solid blue line represents the observed of Si III line and the dotted red line represents the mean GSA. (c) The solid blue line represents the deconvolved He I line and the dotted red lines representing the confidence interval. (d) The solid blue line represents the deconvolved Si III line and the dotted red lines represent the confidence interval.

Nakano, M., Sugitani, K., Watanabe, M., et al. 2012, The Astronomical Journal, 143, 61
Orellana, R., Escárate, P., Curé, M., et al. 2019, A&A, 623, A138
Puls, J., Vink, J. S., & Najarro, F. 2008, Astronomy & Astrophysicsr, 16, 209
Simón-Díaz, S. 2020, in Reviews in Frontiers of Modern Astrophysics; From Space Debris to Cosmology, 155–187
Simón-Díaz, S., Castro, N., Herrero, A., et al. 2011, in Journal of Physics Conference Series, Vol. 328, Journal of Physics Conference Series, 012021
Simón-Díaz, S. & Herrero, A. 2014, A&A, 562, A135
Turner, D. G. 1976, ApJ, 210, 65
Vink, J. S. 2022, Annual Review of Astronomy and Astrophysics, 60, 203
von Zeipel, H. 1924, Monthly Notices of the Royal Astronomical Society, 84, 665
Wiener, N. 1932, Annals of mathematics, 1
Wojdowski, P. S., Schulz, N. S., Ishibashi, K., & Huenemoerder, D. P. 2002, in High Resolution X-ray Spectroscopy with XMM-Newton and Chandra, ed. G. Branduardi-Raymont, 49
Zorec, J. 2023, Galaxies, 11

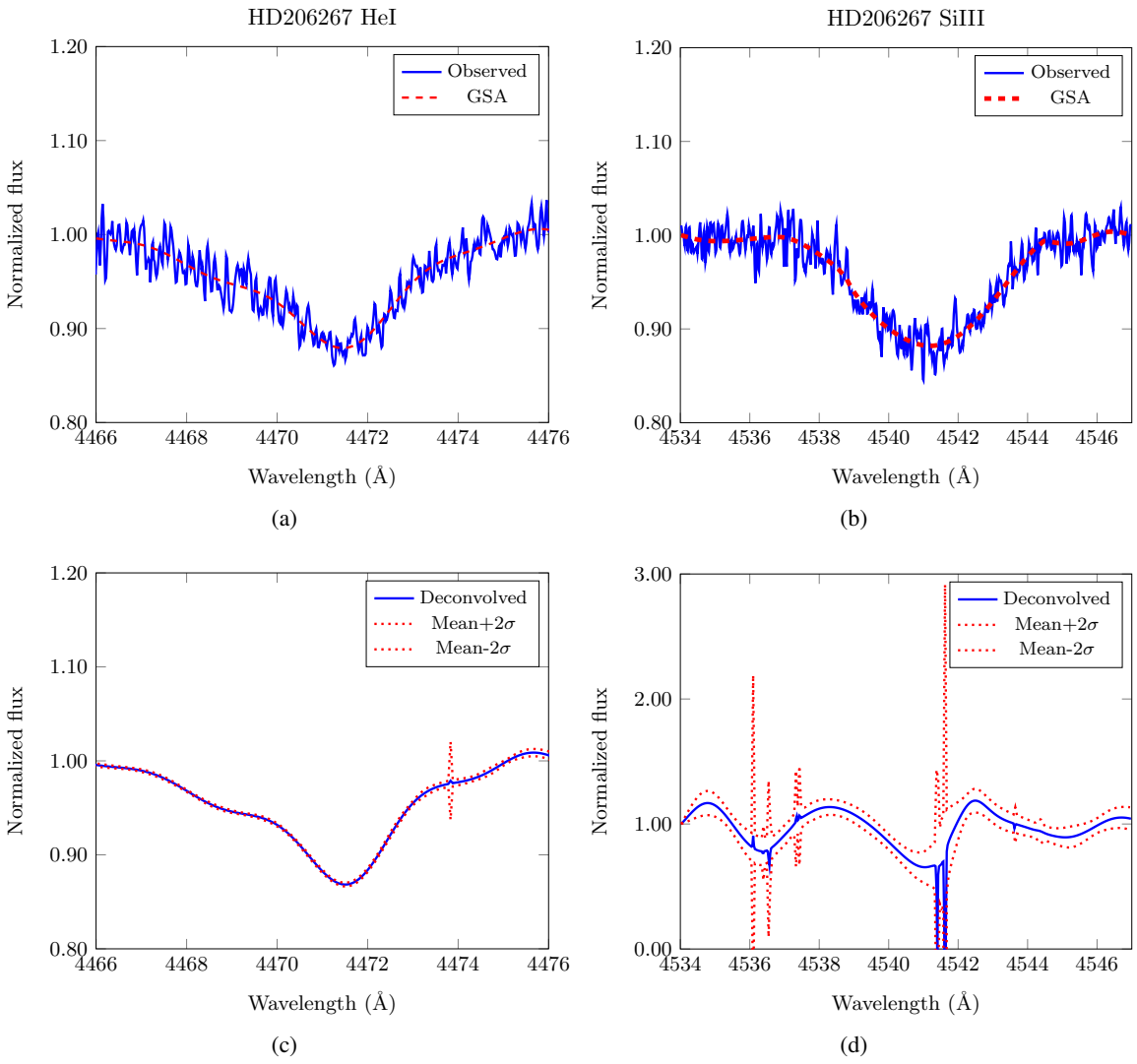

Fig. 5. Deconvolution of two absorption lines for the star HD 206267: (a) The solid blue line represents the observed He I line, and the dotted red line represents the mean GSA. (b) The solid blue line represents the observed Si III line and the dotted red line represents the mean GSA. (c) The solid blue line represents the deconvolved He I line, and the dotted red lines representing the confidence interval. (d) The solid blue line represents the deconvolved Si III line and the dotted red lines represent the confidence interval.

Appendix A: Carrol's expressions in linear and nonlinear limb-darkening laws

In his early works dating back to 1928, Carroll (1928, 1933) stated that the general formulation of a line profile affected by rotational broadening could be achieved through the direct evaluation of the radiative flux considering the following assumptions: (a) that the rotation profile should be symmetric in the line-of-sight and (b) the limb-darkening expression is a separable function of wavelength λ and angle θ. In what follows, let us denote by (ϵ, ω) the first and second limb-darkening coefficients appearing within the limb-darkening expressions, which are slowly varying functions of wavelength λ, temperature and surface gravity.

Thus, from the separability condition, we get the following:

$$I(\lambda, x, y) = I(\lambda, \mu) = I(\lambda + \beta x)\, \phi(\mu), \tag{A.1}$$

where $\mu = \cos\theta = \sqrt{1 - x^2 - y^2}$, with θ representing the angle formed between a point of coordinates (x, y) at the stellar surface and the line-of-sight; $\phi(\mu)$ is the limb-darkening function and $\beta = \lambda\, V \sin i/c$.

The general expression for the outcoming flux from a star affected by rotational broadening is given by:

$$O(\lambda) = K_N \int_{-1}^{+1} I(\lambda, \mu)\, g(x)\, dx, \tag{A.2}$$

where K_N is a normalization factor, and $g(x)$ is a function dependent on the limb-darkening law, namely:

$$g(x) = \int_{-\sqrt{1-x^2}}^{+\sqrt{1-x^2}} \phi(\mu)\, dy \tag{A.3}$$

Appendix A.1: Linear Limb-darkening

The linear limb-darkening law, is given by (see, e.g., Levenhagen 2014, and references therein):

$$\phi(\mu) = 1 - \varepsilon\,(1 - \mu). \tag{A.4}$$

Therefore, Eq. (A.2) reads

$$O(\lambda) = K_N \int_{-1}^{+1} \int_{-\sqrt{1-x^2}}^{+\sqrt{1-x^2}} I(\lambda, \mu)\,(1 - \varepsilon + \varepsilon\cos\theta)\, dy\, dx\,, \tag{A.5}$$

where

$$K_N = \frac{1}{\pi\left(1 - \frac{\varepsilon}{3}\right)}. \tag{A.6}$$

Developing Eq. (A.5) will result in the following integral form:

$$O(\lambda) = \frac{1}{\pi\left(1 - \frac{\varepsilon}{3}\right)} \int_{-1}^{+1} I(\lambda + \beta x) \left[2\,(1 - \varepsilon)\,(1 - x^2)^{1/2} + \frac{\varepsilon\,\pi}{2}\,(1 - x^2)\right] dx\,, \tag{A.7}$$

and the rotational profile $g(x)$ is given by:

$$g(x) = \frac{1}{\pi\left(1 - \frac{\varepsilon}{3}\right)} \left[2\,(1 - \varepsilon)\,(1 - x^2)^{1/2} + \frac{\varepsilon\,\pi}{2}\,(1 - x^2)\right], \tag{A.8}$$

Carroll (1933, see his Eq. 2.2) used $\epsilon = 0.6$.

Appendix A.2: Quadratic Limb-darkening

The quadratic limb-darkening is given by:

$$\phi(\mu) = 1 - \varepsilon\,(1 - \mu) - \omega\,(1 - \mu)^2 \tag{A.9}$$

for which we get the following integral equation:

$$O(\lambda) = K_N \int_{-1}^{+1} I(\lambda + \beta x) \left[2\,(1 - \varepsilon - \omega)\,(1 - x^2)^{1/2} + \frac{\varepsilon\,\pi + 2\,\omega\,\pi}{2}\,(1 - x^2) - \frac{4}{3}\,\omega\,(1 - x^2)^{3/2}\right] dx \tag{A.10}$$

where the normalization constant is:

$$K_N = \frac{1}{\pi\left(1 - \frac{\varepsilon}{3} - \frac{\omega}{6}\right)}\,. \tag{A.11}$$

Finally the function $g(x)$ reads:

$$g(x) = \frac{1}{\pi\left(1 - \frac{\varepsilon}{3} - \frac{\omega}{6}\right)} \left[2\,(1 - \varepsilon - \omega)\,(1 - x^2)^{1/2} + \frac{\varepsilon\,\pi + 2\,\omega\,\pi}{2}\,(1 - x^2) - \frac{4}{3}\,\omega\,(1 - x^2)^{3/2}\right] \tag{A.12}$$

Appendix A.3: Square-root Limb-darkening

The square-root limb-darkening law is given by:

$$\phi(\mu) = 1 - \varepsilon\,(1-\mu) - \omega\,(1-\sqrt{\mu}),, \tag{A.13}$$

and the governing integral equation is given by:

$$O(\lambda) = K_N \int_{-1}^{+1} I(\lambda+\beta x)\left[2\,(1-\varepsilon-\omega)\,(1-x^2)^{1/2} + \frac{\sqrt{\pi}\,\Gamma\,(5/4)}{\Gamma\,(7/4)}\,\omega\,(1-x^2)^{3/4} + \frac{\varepsilon\,\pi}{2}\,(1-x^2)\right]dx \tag{A.14}$$

where the normalization constant is given by:

$$K_N = \frac{1}{\pi\left(1-\frac{\varepsilon}{3}-\frac{\omega}{5}\right)}, \tag{A.15}$$

and $g(x)$ is:

$$g(x) = \frac{1}{\pi\left(1-\frac{\varepsilon}{3}-\frac{\omega}{5}\right)}\left[2\,(1-\varepsilon-\omega)\,(1-x^2)^{1/2} + \frac{\sqrt{\pi}\,\Gamma\,(5/4)}{\Gamma\,(7/4)}\,\omega\,(1-x^2)^{3/4} + \frac{\varepsilon\,\pi}{2}\,(1-x^2)\right], \tag{A.16}$$

where Γ is the Gamma function.

Appendix A.4: Logarithmic Limb-darkening

Finally, the logarithmic limb-darkening law is defined by:

$$\phi(\mu) = 1 - \varepsilon\,(1-\mu) - \omega\,\mu\,\ln\mu\,, \tag{A.17}$$

which gives the integral relation:

$$O(\lambda) = K_N \int_{-1}^{+1} I(\lambda+\beta x)\left[2\,(1-\varepsilon)\,(1-x^2)^{1/2} + \frac{2\,\varepsilon\,\pi + (\ln 4 - 1)\,\pi\,\omega}{4}\,(1-x^2) - \frac{\pi\,\omega}{4}\,(1-x^2)\ln\,(1-x^2)\right]dx \tag{A.18}$$

where the normalization constant is given by:

$$K_N = \frac{1}{\pi\left(1-\frac{\varepsilon}{3}-\frac{2\omega}{9}\right)}, \tag{A.19}$$

and the function $g(x)$ reads:

$$g(x) = \frac{1}{\pi\left(1-\frac{\varepsilon}{3}+\frac{2\omega}{9}\right)}\left[2\,(1-\varepsilon)\,(1-x^2)^{1/2} + \frac{2\,\varepsilon\,\pi + (\ln 4 - 1)\,\pi\,\omega}{4}\,(1-x^2) - \frac{\pi\,\omega}{4}\,(1-x^2)\ln\,(1-x^2)\right] \tag{A.20}$$

Relations (A.7), (A.10), (A.14) and (A.18) can be regarded as convolutions of a non-rotating counterpart profile $I(\lambda+\beta x)$ assuming four different limb-darkening relations and Eqs. (A.8), (A.12), (A.16) and (A.20), with their K_N's, are the corresponding rotational profiles that can be used in Eq. (1).

Appendix B: HD 115842 star

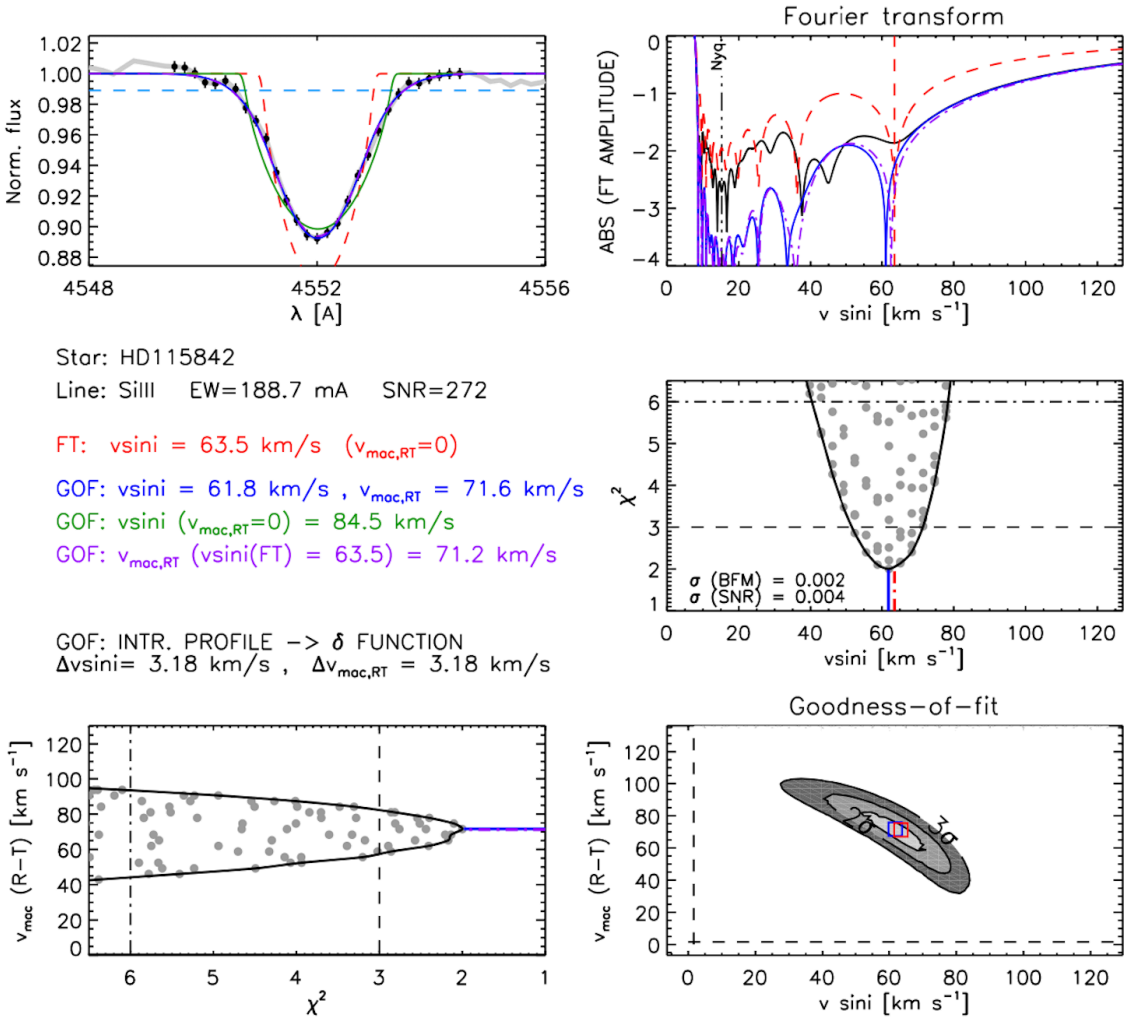

Fig. B.1. Rotational velocity estimation using Iacob-broad tool of HD 115842 star.

Appendix C: HD 47240 star

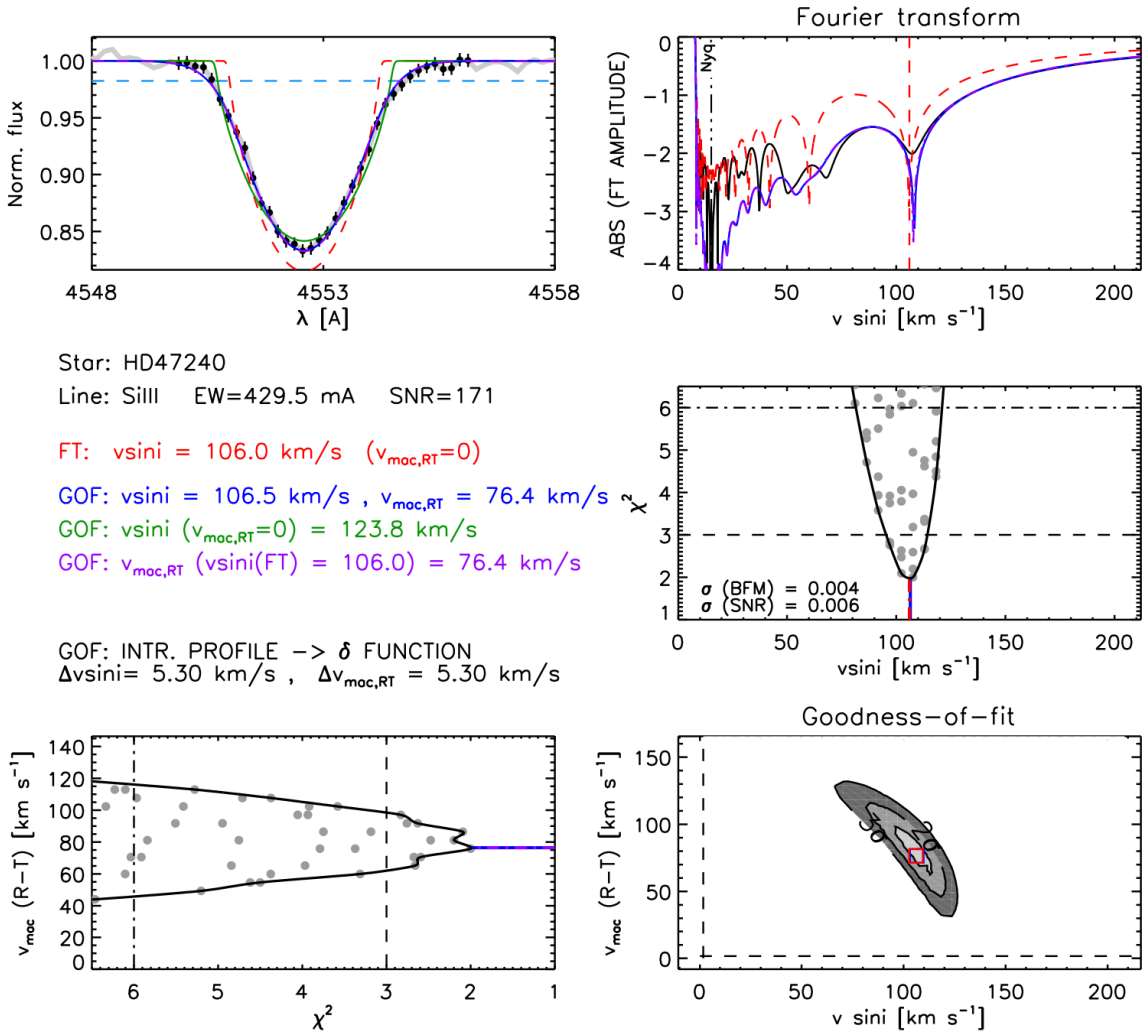

Fig. C.1. Rotational velocity estimation using Iacob-broad tool of HD 47240 star.

Appendix D: HD 206267 star

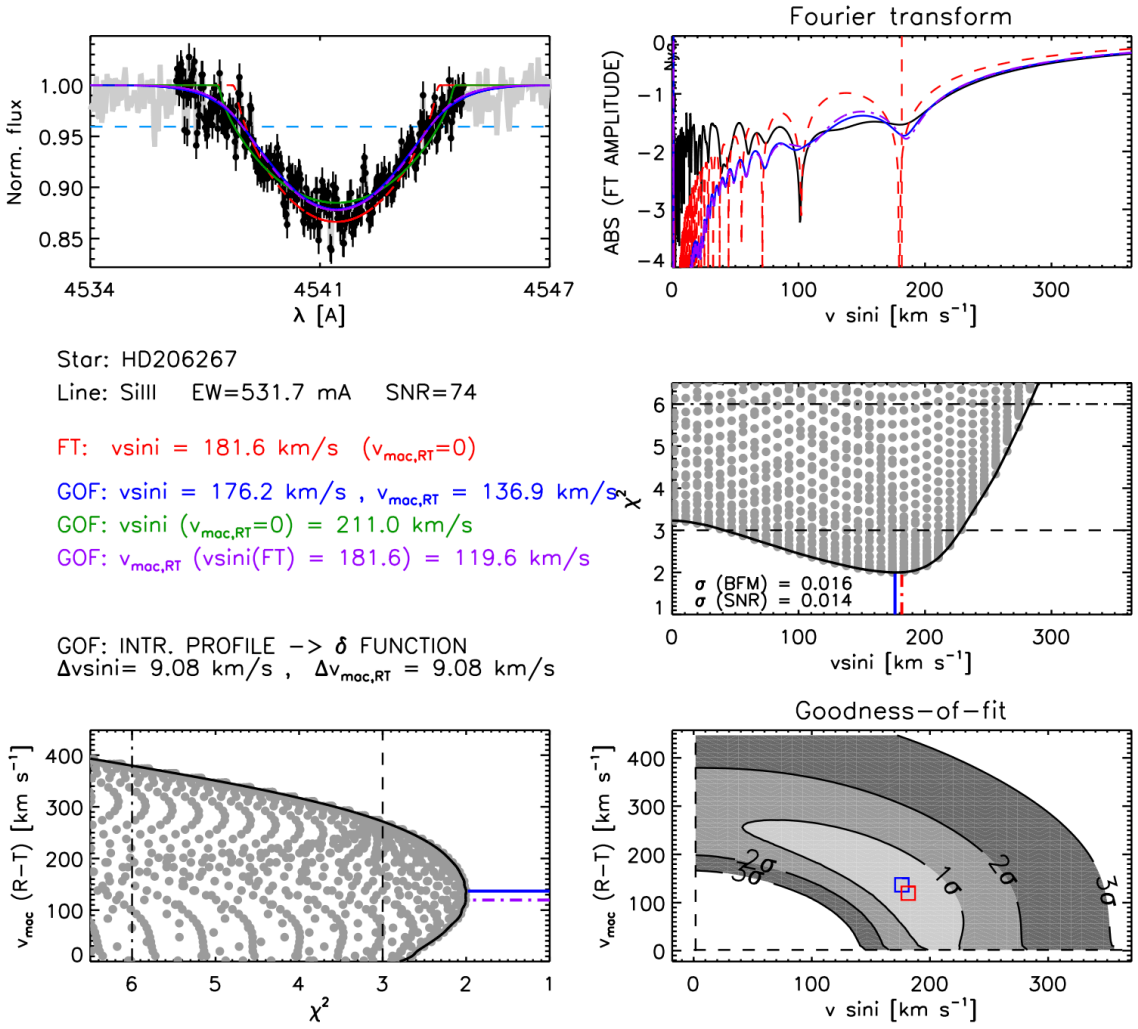

Fig. D.1. Rotational velocity estimation using Iacob-broad tool of HD 206267 star.